

Protodeboronation of Heteroaromatic, Vinyl, and Cyclopropyl Boronic Acids: pH–Rate Profiles, Autocatalysis, and Disproportionation

Paul A. Cox,[†] Andrew G. Leach,[§] Andrew D. Campbell,[‡] and Guy C. Lloyd-Jones^{*,†}

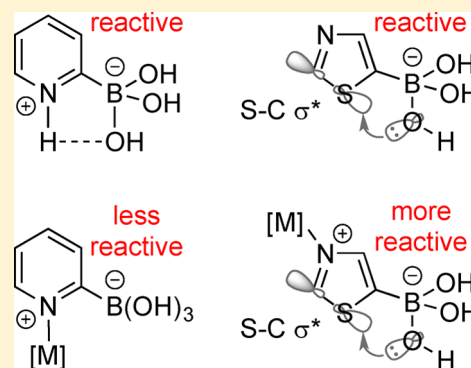
[†]School of Chemistry, University of Edinburgh, Joseph Black Building, David Brewster Road, Edinburgh EH9 3FJ, United Kingdom

[‡]Pharmaceutical Technology and Development, AstraZeneca, Silk Road Business Park, Macclesfield SK10 2NA, United Kingdom

[§]School of Pharmacy and Biomolecular Sciences, Liverpool John Moores University, Byrom Street, Liverpool L3 3AF, United Kingdom

Supporting Information

ABSTRACT: pH–rate profiles for aqueous–organic protodeboronation of 18 boronic acids, many widely viewed as unstable, have been studied by NMR and DFT. Rates were pH-dependent, and varied substantially between the boronic acids, with rate maxima that varied over 6 orders of magnitude. A mechanistic model containing five general pathways (k_1 – k_5) has been developed, and together with input of $[B]_{\text{tot}}$, K_W , K_a , and K_{aH} , the protodeboronation kinetics can be correlated as a function of pH (1–13) for all 18 species. Cyclopropyl and vinyl boronic acids undergo very slow protodeboronation, as do 3- and 4-pyridyl boronic acids ($t_{0.5} > 1$ week, pH 12, 70 °C). In contrast, 2-pyridyl and 5-thiazolyl boronic acids undergo rapid protodeboronation ($t_{0.5} \approx 25$ – 50 s, pH 7, 70 °C), via fragmentation of zwitterionic intermediates. Lewis acid additives (e.g., Cu, Zn salts) can attenuate (2-pyridyl) or accelerate (5-thiazolyl and 5-pyrazolyl) fragmentation. Two additional processes compete when the boronic acid and the boronate are present in sufficient proportions ($\text{pH} = \text{p}K_a \pm 1.6$): (i) self-/autocatalysis and (ii) sequential disproportionations of boronic acid to borinic acid and borane.



INTRODUCTION

Boronic acids are key reagents in synthesis,¹ and ubiquitous in classic processes such as, *inter alia*, Suzuki–Miyaura,² oxidative Heck,³ Chan–Evans–Lam,⁴ and Liebeskind–Srogl couplings,⁵ and addition to enones,⁶ carbonyls, and imines.⁷ Boronic acid decomposition, notably by *in situ* protodeboronation,¹ compromises reaction efficiency, and motifs such as 2-heteroaryl,⁸ vinyl,⁹ and cyclopropyl¹⁰ are sometimes troublesome. As a consequence, a range of techniques have been developed to mitigate decomposition during coupling:^{1,11} these include highly tuned catalysts,¹² the use of additives (e.g., Cu, Zn, and Ag salts) sometimes proposed to act by transmetalation,¹³ masked reagents,¹⁴ and slow release of the boronic acid *in situ*¹¹ from MIDA boronates¹⁵ and trifluoroborates.¹⁶

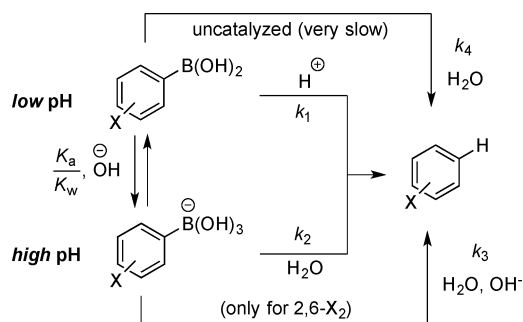
Given the importance of boronic acids in Suzuki–Miyaura coupling, a process that is frequently conducted in aqueous–organic solvent media,^{16c} general mechanistic understanding of direct aqueous protodeboronation is surprisingly limited. Moreover, nearly all studies have focused on substituted phenylboronic acids.^{1,12,17} The most detailed investigation was reported by Kuivila, who measured the protodeboronation kinetics of a series of $\text{ArB}(\text{OH})_2$ species ($\text{Ar} = o,m,p\text{-X-C}_6\text{H}_4$; $\text{X} = \text{MeO}, \text{Me}, \text{Cl}, \text{and F}$) in aqueous buffers at 90 °C, with initial $\text{ArB}(\text{OH})_2$ concentrations in the range 3–5 mM.^{17c–f} By

analysis of pH–rate profiles (between pH 1.0 and 6.7), two pathways were identified, Scheme 1. The first was a specific acid-catalyzed process (k_1), shown to proceed via aromatic electrophilic substitution of B by H. The second pathway was found to be base-catalyzed, and proposed to proceed via hydrolysis (k_2) of the boronate anion ($[\text{ArB}(\text{OH})_3]^-$). This latter species is generated in a pH-determined equilibrium involving association of water (K_a)¹⁸ or hydroxide (K_a/K_W) with the boronic acid. A key issue is that the kinetics were measured by UV–vis spectroscopy and could not be determined above pH 6.7 due to the onset of UV-dominating boronic acid oxidation processes.^{17f} As a consequence of the pH being substantially below that required to effect significant conversion of the boronic acid to the boronate, the rate constant (k_2) was calculated from k_{obs} , using an estimated value for K_a . In addition to the elucidation of the two major pathways (k_1 and k_2) for aqueous protodeboronation, Kuivila’s studies also identified that electron withdrawing groups, at *para* or *meta* positions on the aromatic ring, attenuate protodeboronation rates, via both pathways. However, while these studies were extensive,^{17c–f} they were conducted long before the ascendancy of the Suzuki–Miyaura reaction.² In other words, the

Received: March 30, 2016

Published: June 29, 2016

Scheme 1. Kuivila Mechanisms (k_1 , k_2) for $\text{ArB}(\text{OH})_2$ Protodeboronation in Aqueous Acidic (k_1)^{17c} and Basic (k_2)^{17f} Media^a



^aAlso shown is a third pathway, involving boronate $[\text{ArB}(\text{OH})_3]^-$ deprotonation and C–B protolysis (k_3), proposed by Perrin^{17k} for substrates with 2,6-disubstitution ($X = \text{F}, \text{Cl}, \text{Br}, \text{CF}_3$), and an uncatalyzed pathway (k_4) involving direct reaction with (autoionized) water.

importance of detailed study of the base-catalyzed process, across the full alkaline pH range (i.e., well above pH 6.7), was not yet apparent.

Indeed, it was only rather recently that the kinetics of protodeboronation of arylboronic acids have been studied under basic conditions. In 2002, Frohn measured protodeboronation rates of various polyfluorophenyl boronic acids in aqueous pyridine, and in aqueous basic methanol, concluding that the mechanism involved protolysis of either the boronate (i.e., k_2) or the conjugate base of the boronic acid.¹⁷ⁱ In 2003 Cammidge reported in detail on the effect of various anhydrous and aqueous–organic media in the protodeboronation of 2,3-difluoro-4-heptyl-6-tolyl boronic acid mediated by CsF ,^{17j} concluding that aqueous protolysis of the corresponding boronate was involved. In 2010 Buchwald used calorimetry to measure protodeboronation kinetics of a series of substituted 2,6-difluorophenyl boronic acids (3-F, 3-OBu, 4-F, and 4-H) in a biphasic basic aqueous medium (aq $\text{K}_3\text{PO}_4/\text{THF}$).¹² Perrin extended this study, including other electronegative 2,6-disubstituents, Cl, Br, and CF_3 ,^{17k} which led to the proposal of a new, i.e., non-Kuivila type, mechanism involving specific-base-mediated protolysis (k_3) of the boronate anion ($[\text{ArB}(\text{OH})_3]^-$). The process was reported to only occur with boronic acids bearing a substituent at both *ortho*-positions (i.e., 2,6-disubstitution).^{17k}

Despite the core role of heteroaromatic boronic acids in synthesis and discovery, and the propensity for many to undergo protodeboronation, during storage¹⁷ⁱ and in coupling,^{8,12} there is a near-complete absence of the kinetic data requisite for their behavior to be compared and contrasted. Thus, while it is known empirically, or anecdotally, that certain heteroaromatic boronic acids are much more prone to protodeboronation than others,^{1,8,11b} it is not clear whether overall they behave similarly to substituted phenylboronic acids, i.e., displaying the simple acid- and base-catalyzed pH relationships (k_1 , k_2) identified by Kuivila, or whether there are more complex pH dependencies for some classes of heteroaromatic boronic acids, for example involving heterocycle basicity, or other pathways, such as the specific-base-mediated protolysis (k_3) identified by Perrin.^{17k} Indeed, it is not even clear for an individual class of heteroaromatic boronic acid

whether extremes of pH (low or high) are to be avoided, or are beneficial, in terms of stability.

For all of the above reasons, we set out to study the intrinsic aqueous protodeboronation of a range of heteroaromatic (2–17), vinyl (18), and cyclopropyl (19) boronic acids, in a homogeneous organic–aqueous medium. Herein, we report the overall kinetics of their protodeboronation, but more importantly also show how the resulting pH–rate profiles can be simulated and analyzed using a general kinetic model. The model extends beyond the basic Kuivila processes (k_1 , k_2), by including the Perrin mechanism (k_3), plus three additional protolysis processes ($k_{2\text{cat}}$, k_4 and k_5 , *vide infra*), the requisite pH-dependent speciation equilibria for boronic acid association with water (K_a), and, if required, the protonation state of basic heterocycles (K_{aH}). The model can be used in two ways: (i) as a general exploratory tool, with manual input of the requisite pH, concentrations, rates, and equilibrium constants, or (ii) as a means to fit experimental data, through automated numerical iteration of rate and equilibrium constants (including K_a and K_{aH}), provided that the rate data has been acquired over a suitably wide pH range. To assist in application of the model, a preconfigured spreadsheet is provided as part of the [Supporting Information](#).

The model provides the basis for quantification of the dominant protodeboronation processes occurring for different boronic acid species, at different pH and substrate concentrations. Thus, the impact of pH on the kinetics allows identification of new mechanistic regimes, and these mechanisms can then be explored in more detail using kinetics, isotopic labeling, effects of additives, and computation. Overall the study has facilitated the following: (i) classification of the reactivity imparted by 16 different heterocyclic structures (2–17) between pH 1 and 13; (ii) elucidation and investigation of new protodeboronation mechanisms and a competing disproportionation process; (iii) preliminary details on origins of the (de)stabilizing effect of additives such as Zn and Cu salts on some heterocyclic boronic acids; and (iv) identification of substrate-specific pH-stability zones, in which even notoriously unstable boronic acids, e.g., 2-pyridyl, can be stable for a few hours at 70 °C. This information will aid a more informed choice of conditions for the preparation, storage,¹⁷ⁱ and application of boronic acids in synthesis,¹ as well as a means to induce their deliberate¹⁹ protodeboronation.

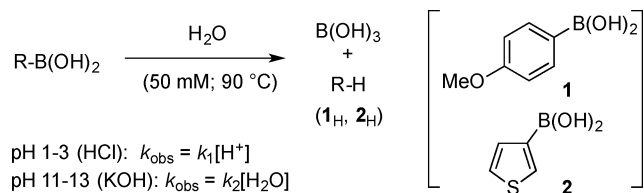
RESULTS AND DISCUSSION

1. Protodeboronation via Kuivila Mechanisms (k_1 and k_2)

In preliminary studies we confirmed that the protodeboronation of a simple *para*-substituted phenyl boronic acid could be satisfactorily analyzed *in situ* by $^1\text{H}/^{11}\text{B}$ NMR under aqueous conditions. With *p*-anisyl boronic acid (**1**),^{17c,f} protodeboronation kinetics were determined in water at 90 °C, without a malonate buffer.^{17c,f} The aqueous association constant ($\text{p}K_a$ **1** = 9.10; 90 °C) was determined by ^{11}B NMR pH titration. Control experiments confirmed that basic solutions of **1** became pale brown in color, with large increases observed in UV–vis absorption spectra, as reported by Kuivila.^{17f} However, the NMR spectra of such samples were unaffected: there was no sign of mequinol (*p*-hydroxy anisole), the anticipated product of oxidation of **1**, or indeed anything other than the time-average signal from $[\text{1}/1_{\text{OH}}]$ and the protodeboronation products, anisole and boric acid. The trace quantities of oxidative side product(s) are thus intensely UV-active, and possibly polymeric.

Using HCl and KOH to explore the acid (pH 1–3) and base (pH 11–13) regimes, protodeboronation kinetics were analyzed by nonlinear regression of the exponential decays observed for $[1/1_{\text{OH}}]$. The second-order rate constants (k_1 and k_2) are given in Table 1, entry 1. Kuivila's value for the limiting

Table 1. Protodeboronation 1 and 2 at 90 °C



| entry | ArB(OH) ₂ | pK _a ^a | k ₁ M ⁻¹ s ⁻¹ | k ₂ M ⁻¹ s ⁻¹ |
|----------------|----------------------|------------------------------|--|--|
| 1 | 1 | 9.10 | 0.68 × 10 ^{-4b} | 3.9 × 10 ^{-8b} |
| 2 ^c | 1 | 9.60 ^d | 1.1 × 10 ^{-4e} | 8.4 × 10 ^{-6f} |
| 3 | 2 | 8.91 | 3.3 × 10 ^{-6b} | 1.4 × 10 ^{-8b} |

^a¹¹B NMR pH titration. ^b¹¹B NMR at pH 1–3 and 11–13. ^cFrom refs 17c and f. ^dEstimated in ref 17f. ^eExtrapolated from data in ref 17c. ^fFrom k_{obs} at pH 6.7 (25 °C, uncorrected) and estimated K_a.

rate constant at high pH (k_2 , entry 2) was obtained by pH–rate extrapolation and is 2 orders of magnitude too large.^{17k} This arises from the conflation of an overestimated pK_a for 1 (9.60), with an uncorrected pH (25 °C)²⁰ for the k_{obs} determination at 90 °C, and reinforces the value of full pH range rate profiling.

Moving to the protodeboronation of heterocycles, 3-thienylboronic acid (2) was chosen for initial studies, on the basis of its solubility, relative stability, and low basicity. Second-order rate constants (k_1 and k_2 ; Table 1, entry 3) were determined under the same conditions (50 mM, H₂O, 90 °C) as for *p*-anisyl boronic acid 1. Within the limits of the pH range explored (pH 1–13), there was no detectable contribution by the base-catalyzed boronate mechanism (k_3), or direct reaction of the boronic acid with H₂O (k_4 ; Scheme 1),²¹ although both mechanisms (k_3 and k_4) were found to be important with some heterocycles, *vide infra*.

3-Thienyl boronic acid 2 is less susceptible to aromatic electrophilic substitution (k_1)²² than 1, but the boronates (1_{OH} and 2_{OH}) are of similar reactivity (k_2 , Table 1, entries 1 and 3). Computational studies on this process identified rate-limiting C-protonolysis of the boronate (2_{OH}, Figure 1, upper structure) by water. As found for all of the boronates studied, the three hydroxyl groups in 2_{OH} preferentially adopt a distinctive triskelion conformation. Hydrogen bonding of the boronate by incoming water results in the C–B bond stretching such that, in the transition state (TS), the 3-thienyl carbanion is midpoint in its translation from the Lewis acid (B(OH)₃) to the Brønsted acid (OH).

2. Autocatalyzed Protodeboronation ($k_2\text{cat}$). If protodeboronation of 2 arises solely by the Kuivila mechanisms (k_1 , k'_2), ($k'_2 = k_2[\text{H}_2\text{O}]$) the empirical rate equation predicts a simple pH–log k_{obs} rate profile, Figure 2. Specifically, for k'_2 (see solid line, Figure 2), the rate should rise and then reach a plateau as the pH extends above the pK_a of the boronic acid 2 (pK_a = 8.91 at 90 °C). The data deviates from this theoretical curve, with the deviation being greatest at pH 8.9. This deviation was found for many of the boronic acids studied, *vide infra*, and indicates that there is an additional protodeboronation process that augments k'_2 , but with a distinctly different pH profile. A pronounced concentration dependence was

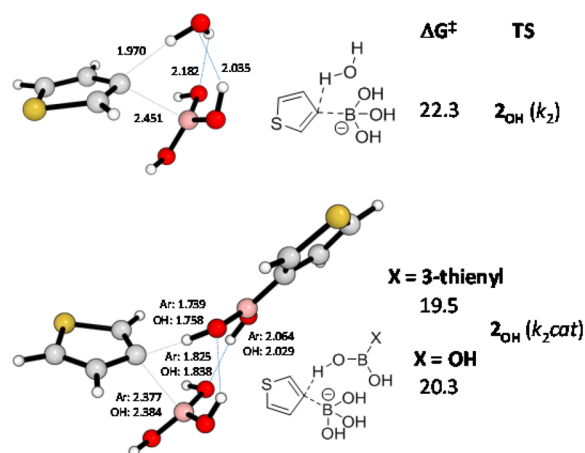


Figure 1. DFT (M06L/6-311++G**) transition state structures for protonolysis of 3-thienylboronate 2_{OH} by water (k_2 , top) and by boronic acid (2, $k_2\text{cat}$, bottom) to generate 2_H and [B(OH)₄]⁻. Distances are shown in Å and free energies are given in kcal/mol.

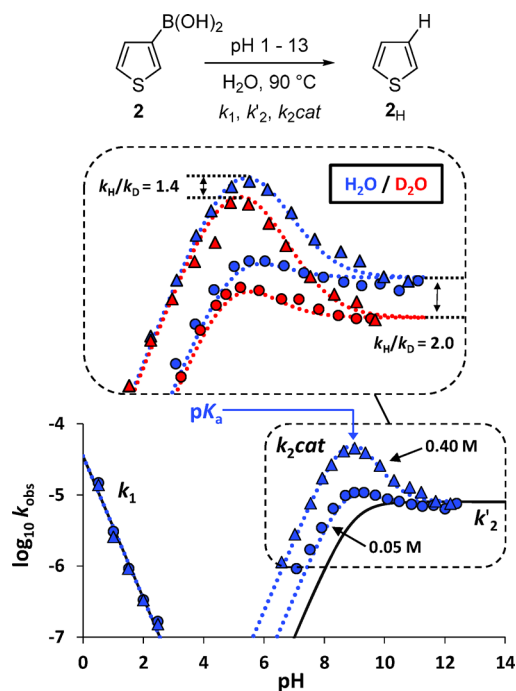


Figure 2. Effect of pH and concentration on the rate of protodeboronation of thienyl boronic acid 2. Dashed lines: $k_{\text{obs}} = ((k'_2 + k_2\text{cat}[\text{B}]_{\text{tot}})/(1 + 10^{(\text{pK}_a - \text{pH})})) + ((k_1/10^{\text{pH}})/(1 + 10^{(\text{pH} - \text{pK}_a)}))$ values as Table 1, entry 3, plus $k_2\text{cat} = 6.2 \times 10^{-5} \text{ M}^{-1} \text{ s}^{-1}$; for solid line, $k_2\text{cat} = 0$. Inset shows rate profile in D₂O (red), using an x-axis scale of $\text{pD} + \Delta\text{pK}_w$ to account for the change in water autoionization (K_w).³⁰ pK_a 2 (¹¹B NMR pH titration, 90 °C): 8.91 (H₂O) and 9.68 (D₂O).

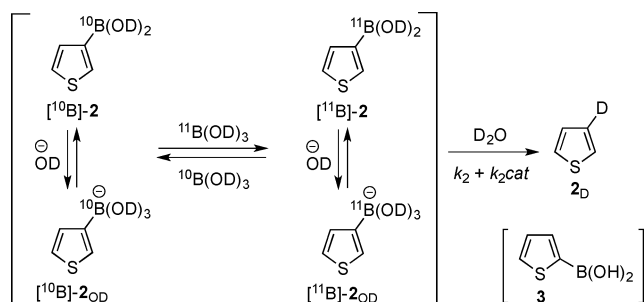
noted, with the deviation from k'_2 becoming greater as the boronic acid concentration is raised (compare 0.05 to 0.40 M, Figure 2). As the maximum deviation occurs when pH = pK_a (8.91), where the proportions of [RB(OH)₃]⁻ and RB(OH)₂ are identical, analogous to that of a bimolecular Job-plot,²⁸ this suggests self-catalysis ($k_2\text{cat}$). To account for the approximately pseudo-first-order kinetics (*vide infra*), the product (B(OH)₃) needs to be a similarly effective autocatalyst,²⁹ as the boronic acid is a self-catalyst.^{17l} This was confirmed by addition of 350 mM ¹⁰B(OH)₃ to the protodeboronation of 50 mM 2. At pH

8.90, ^{11}B NMR analysis afforded the same pseudo-first-order rate constant as for 400 mM **2** alone ($[\text{B}]_{\text{tot}} = 400 \text{ mM}$ in both cases). Using an augmented rate equation containing $k_{2,\text{cat}}$ allows satisfactory kinetic simulations (dashed lines in Figure 2). DFT transition state energies confirmed that water can be replaced by boronic acid **2** (Figure 1, lower structure) or boric acid as proton sources, and KIEs determined from reactions in D_2O (Figure 2, inset) confirm rate-limiting proton-transfer.

3. B–OH-Catalyzed Disproportionation. After some preliminary investigation with heterocyclic boronic acids, a mixture of $\text{H}_2\text{O}/1,4\text{-dioxane}$ (1:1) at 70°C was found to provide the best combination of substrate solubility (50 mM) while remaining fully homogeneous at the wide range of base, salt, buffer, additive, and acid concentrations required to usefully explore the pH range (1–13). With higher initial concentrations of boronic acid, some substrates displayed small deviations from pseudo-first-order protodeboronation kinetics when carefully monitored at $\text{pH} = \text{p}K_{\text{a}} \pm 0.1$.

This deviation had already been observed with thienyl boronic acid **2** in H_2O at 90°C , *vide supra*, and together with tests for boryl exchange at the aryl ring, Scheme 2, indicated that processes in addition to $k_{2,\text{cat}}$ occur when both $[\text{RB}(\text{OH})_3]^-$ and $\text{RB}(\text{OH})_2$ are present at high concentration ($\text{pH} = \text{p}K_{\text{a}}$).

Scheme 2. $^{10}\text{B}/^{11}\text{B}$ Exchange: Reaction of $^{11}\text{B}(\text{OD})_3$ (0.2 M) with ^{10}B -2** (0.2 M) To Generate Small Quantities of ^{11}B -**2**/ ^{11}B -**2** $_{\text{OD}}$ and $^{10}\text{B}(\text{OD})_3$ ($^{10}/^{11}\text{B}$ NMR, D_2O , 90°C)^a**



^aRegioisomer **3** protodeboronates without significant disproportionation.

^{11}B NMR analyses of this process indicated other transient minor ($\leq 5\%$) species to be present, and the pH-shift dependency of one of these species suggested it to be a borinate,³¹ $[(3\text{-thienyl})_2\text{B}(\text{OH})_2]^-$, generated by disproportionation of **2**/**2** $_{\text{OH}}$. Regioisomeric 2-thienyl boronic acid (**3**) was found to undergo much faster protodeboronation (k_2 and $k_{2,\text{cat}}$) than 3-thienyl **2**, with no significant disproportionation. In contrast, 2-furyl boronic acid (**4**, 1:1 $d_8\text{-dioxane}/\text{D}_2\text{O}$, 0.5 equiv of KOD; $\text{pD} = \text{p}K_{\text{a}}$) underwent disproportionation faster than protodeboronation when the concentration was raised to 0.4 M, Figure 3.

The temporal evolution (^1H NMR) indicated a two stage process, initially giving difurylborinic acid ($\text{R}_2\text{B}(\text{OD})$), which disproportionates further to give the trifurylborane (R_3B , Figure 3). Over a period of days, all species protodeboronate, directly or indirectly, to give boric acid and furan (**4** $_{\text{D}}$).³³ DFT studies investigated a number of mechanisms for the aryl transfer between the boron centers. These included an analogue of the autocatalysis mechanism, Figure 1, TS **2** $_{\text{OH}}$ ($k_{2,\text{cat}}$), in which the furyl anion transfers to the Lewis acid B, rather than Brønsted

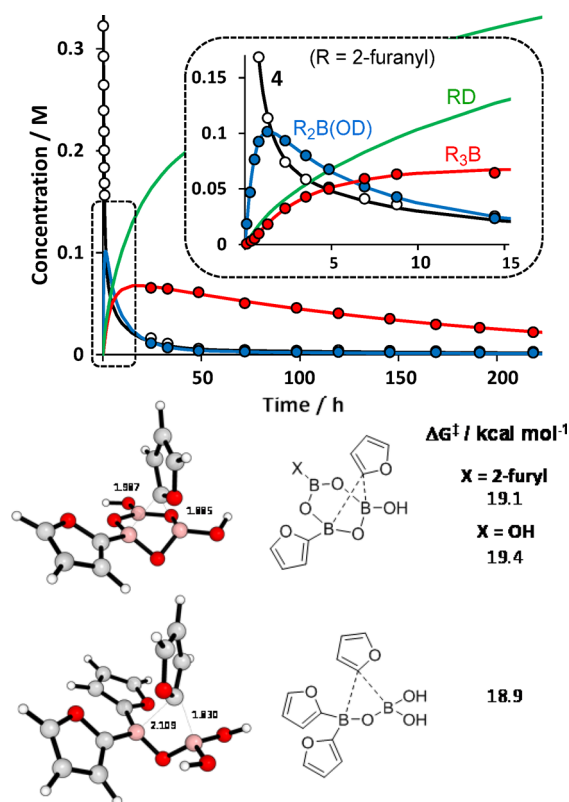


Figure 3. Upper: temporal concentration data for disproportionation of 2-furyl boronic acid **4** (1:1 $d_8\text{-dioxane}/\text{D}_2\text{O}$, 0.5 equiv of KOD, 70°C). Circles: data. Solid lines: simulation (see SI for details). $^2\text{H}_1\text{-furan}$ ($\text{RD} = \text{4}_{\text{D}}$) is volatile under the reaction conditions and was not monitored. Lower: transition states (DFT) for disproportionation to difurylborinic acid and trifurylborane.³²

acid H, in an H-bonded $[\text{4} + \text{4}_{\text{OH}}]$ intermediate. However, the computed barrier for transfer to B (22.5 kcal/mol) is greater than that for H (20.3 kcal/mol), and protodeboronation would dominate if solely these isomeric transition states are operative. An alternative process was therefore considered in which a cyclic boroxine-ate complex (Figure 3, X = furyl or OH, upper structure) facilitates aryl-migration across the ring. The rate-limiting barriers for aryl migration are computed to be 19.1–19.4 kcal/mol for 2-furyl **4** $_{\text{OH}}$ and 19.5–19.9 kcal/mol for 3-thienyl **2** $_{\text{OH}}$.

Accurately computing free energies in solution for very different processes is challenging; nonetheless, the calculations suggest that migration dominates over protodeboronation for 2-furyl **4**, while the opposite is the case for 3-thienyl **2**. The transition state structures suggest an electronic and steric component to this preference. Mulliken charges indicate the nonmigrating 2-furyl bears a larger negative charge than the equivalent group for 3-thienyl. Further, the preferred conformation of the transition state places the migrating group in close proximity to the other aromatic ring; larger rings or those with C–H groups adjacent to the boronic acid group will inevitably involve steric clashes, even more so when X = aryl. The subsequent step leading to triarylborane requires reaction of a borinic with a boronic acid and thus cannot involve a cyclic boroxine. Instead it is computed to proceed via a transition state involving a dimer (Figure 3, lower structure). The free energy barrier (+18.9 kcal/mol) is comparable to that for the first step, and thus consistent with the observed

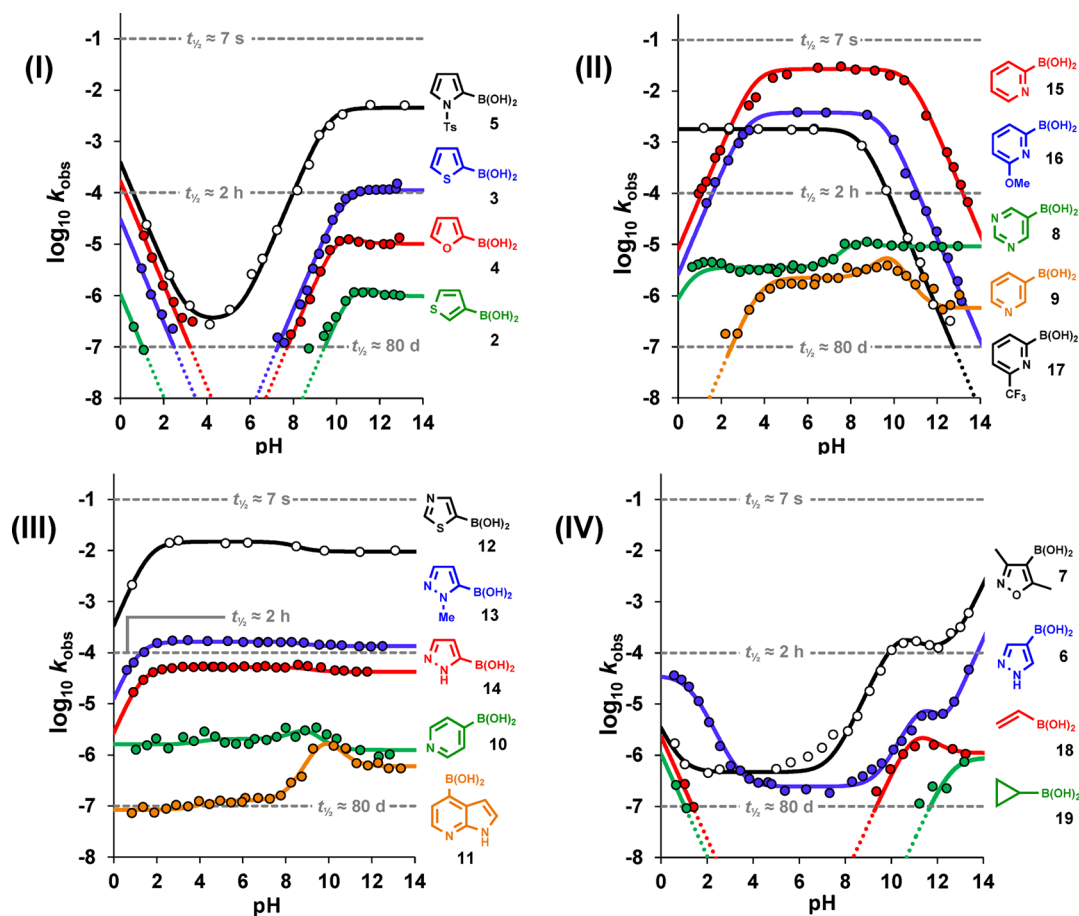


Figure 4. pH–rate profiles (I–IV) for pseudo-first-order protodeboronation ($k_{\text{obs}}/\text{s}^{-1}$) of boronic acids 2–19 in 1:1 $\text{H}_2\text{O}/1,4$ -dioxane at 70°C . Reactions analyzed *in situ* by ^{11}B NMR were conducted in quartz NMR tubes to avoid $[\text{B}(\text{OH})_4]^-$ release from borosilicate NMR tubes. Circles: experimental data. Solid lines: simulation using model (Figure 5) with data from Table 2. Rates below $\log k_{\text{obs}} = -7$ are not modeled.

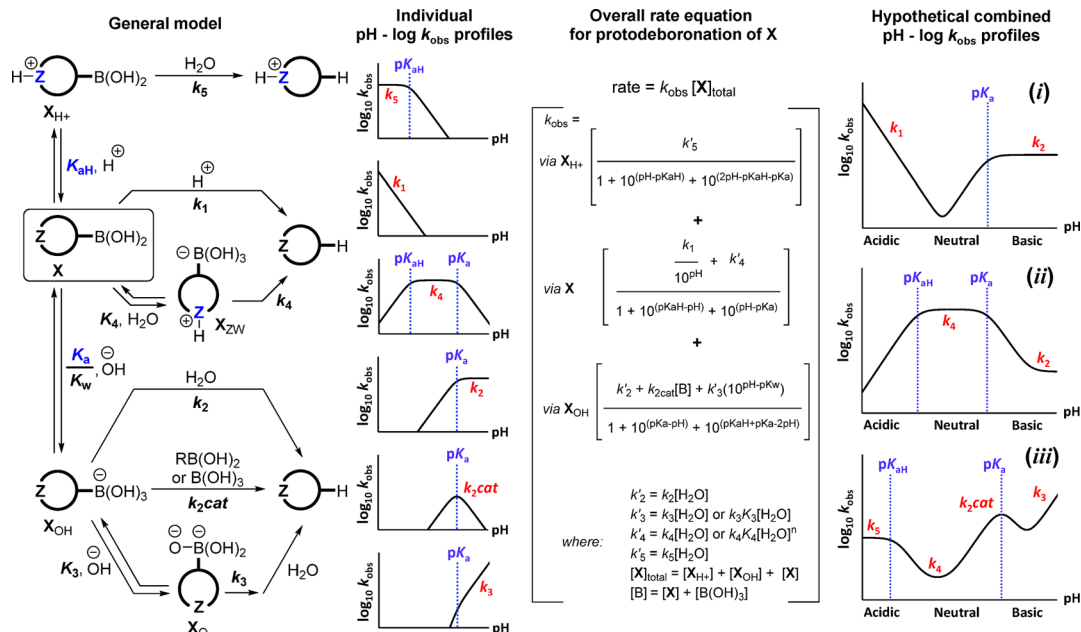
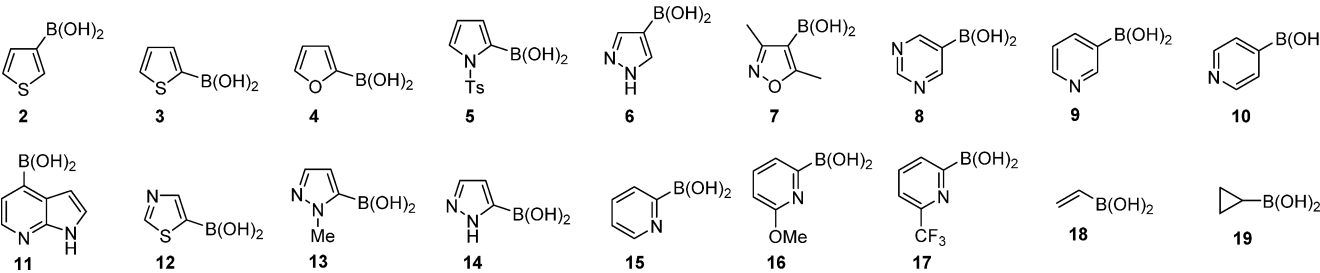


Figure 5. General model for heterocycle protodeboronation (Z = basic nitrogen), individual pH– $\log k_{\text{obs}}$ profiles, overall rate equation based on the three-state speciation [neutral (X), N -protonated (X_{H^+}), and boronate (X_{OH})], and example combined pH– $\log k_{\text{obs}}$ profiles (i, ii, iii).

transient accumulation of diarylborinic acid. Using these models for reversible furyl transfer, with an irreversible

Table 2. Equilibrium and Rate Constants Employed in the pH Simulation (See Overall Rate Equation in Figure 5) for Protodeboronation of Heteroaromatic, Vinyl, and Cyclopropyl Boronic Acids 2–19 in 1:1 H₂O/1,4-Dioxane at 70 °C



Chemical structures of boronic acids 2–19 are shown above the table. Structures 2–10 are heteroaromatic boronic acids. Structures 11–17 are heterocyclic boronic acids. Structure 18 is a vinyl boronic acid, and structure 19 is a cyclopropyl boronic acid.

| entry | RB(OH) ₂ | pK _{aH} ^a | pK _a ^b | log k ₁ | log k' ₂ ^c | log k _{2cat} | log k' ₃ ^e | log k' ₄ | log k' ₅ |
|-------|---------------------|-------------------------------|------------------------------|---------------------|----------------------------------|-----------------------|----------------------------------|---------------------|---------------------|
| 1 | 2 | | 11.04 | -5.95 | -6.01 | -4.21 | ≤-5.32 ^d | | |
| 2 | 3 | | 10.38 | -4.44 | -3.92 | ≤-3.54 ^d | ≤-3.07 ^d | | |
| 3 | 4 | | 10.29 | -3.71 | -4.98 | -3.32 | ≤-4.12 ^d | | |
| 4 | 5 | | 9.64 ^c | -3.41 | -2.34 | ≤-2.07 ^d | ≤-1.93 ^d | -6.48 | |
| 5 | 6 | 1.26 (1.70) | 11.61 | -3.16 | ≤-6.02 ^d | -3.27 | -3.72 | -6.60 | ≤-5.68 ^d |
| 6 | 7 | 0.04 ^e (<0.50) | 10.45 | -5.51 | -4.01 | -2.00 | -2.62 | -6.38 | ≤-4.61 ^d |
| 7 | 8 | 0.14 ^e (<0.60) | 8.18 | ≤-4.82 ^d | -5.04 | -3.44 | ≤-4.75 ^d | -5.44 | ≤-4.83 ^d |
| 8 | 9 | 3.60 (4.22) | 9.76 | ≤-3.10 ^d | -6.05 | -3.60 | ≤-5.59 ^d | -5.71 | ≤-6.70 ^d |
| 9 | 10 | 3.36 ^e (3.82) | 8.94 | ≤-3.76 ^d | -5.93 | -3.78 | ≤-5.78 ^d | -5.71 | -5.77 |
| 10 | 11 | 2.95 ^e (3.41) | 9.90 | ≤-5.64 ^d | -6.24 | -3.95 | ≤-6.60 ^d | -6.89 | -7.07 |
| 11 | 12 | 1.62 (1.85) | 8.41 ^c | ≤-2.60 ^d | -2.02 | ≤-1.58 ^d | ≤-2.21 ^d | -1.83 | ≤-4.22 ^d |
| 12 | 13 | 1.08 (1.62) | 8.82 | ≤-4.22 ^d | -3.87 | -3.49 | ≤-3.94 ^d | -3.78 | ≤-5.31 ^d |
| 13 | 14 | 1.36 (2.00) | 9.11 | ≤-4.58 ^d | -4.35 | -3.19 | ≤-3.93 ^d | -4.28 | ≤-5.84 ^d |
| 14 | 15 | 3.52 (3.86) | 10.76 ^c | ≤-0.74 ^d | ≤-4.26 ^d | ≤-0.67 ^d | ≤-3.74 ^d | -1.60 | ≤-4.24 ^d |
| 15 | 16 | 3.16 (3.60) | 9.54 ^c | ≤-1.36 | ≤-6.72 ^d | ≤-2.33 ^d | ≤-6.04 ^d | -2.41 | ≤-4.52 ^d |
| 16 | 17 | -1.06 ^e (<-0.6) | 8.49 ^c | ≤-2.06 ^d | ≤-6.32 ^d | ≤-1.84 ^d | ≤-4.82 ^d | -2.75 | ≤-0.06 ^d |
| 17 | 18 | | 11.21 | -5.57 | -6.02 | -3.90 | ≤-5.73 ^d | | |
| 18 | 19 | | 12.72 | -5.95 | -6.01 | -5.01 | ≤-5.91 ^d | | |

^apK_{aH} in parentheses determined by ¹H NMR pH titration at 25 °C; pK_{aH} at 70 °C from iterative fitting of rate data (unless stated). ^bpK_a by ¹¹B NMR pH titration at 70 °C (unless stated). ^cpK_a from iterative fitting of rate data. ^dThis value is not required for satisfactory simulation; greater values induce ≥5% change in the sum of square errors between simulation and data across the overall pH profile. ^epK_{aH} fixed at empirical offset (-0.46 units) based on entries 5, 8, 11–16. ^fDue to the pK_{aH} of 17 being <-1.06, this value is a substantial overestimate.

protodeboronation, predominantly via the boronic acid, a good fit to the experimental data was achieved by kinetic simulation (solid lines, Figure 3).

4. General Model for Protodeboronation Kinetics.

With suitable conditions established for analysis (50 mM substrate, 1:1 H₂O/1,4-dioxane, 70 °C) the pseudo-first-order kinetics (*k*_{obs}) of reactions of boronic acids 2–19 were measured as a function of pH (1–13), Figure 4, profiles I–IV, see SI for full details. Rates were pH-dependent, and varied substantially between the boronic acids, with rate maxima that varied over 6 orders of magnitude (half-lives ranging from seconds to weeks). For some substrates, specific pH ranges reduced the protodeboronation rates to such an extent that, for reasons of accuracy, they were omitted from the log(*k*_{obs})-pH analyses. An arbitrary threshold of log *k*_{obs} ≥ 7.0 (half-life ≤ 80 days) was set for data inclusion (see dashed lines in profiles I–IV, Figure 4).

To analyze the pH-dependency of the protodeboronation reactions of heterocyclic boronic acids, we developed a general model, Figure 5. Aiming to keep as minimal a model as required, we began with the Kuivila processes, and added further processes, when necessary, as the analysis of heterocyclic boronic acids 2–17 evolved. To simplify the discussion, the overarching model is presented in advance of the analysis of the protodeboronation characteristics of 2–17. As many of the heterocyclic systems studied are basic, the model includes, when appropriate, the pK_{aH} of the N-

protonated form of the heterocycle, in addition to the pK_a for aqueous association at boron.

The kinetics are determined by a 3-fold speciation of the boronic acid (X): as an N-protonated form (X_{H+}; only for 6–17), a neutral form (X), and a boronate form (X_{OH}). Specific protodeboronation processes occur from the three speciation states. For the neutral form (X), there is the acid-catalyzed Kuivila process (*k*₁), and a pH-independent direct reaction with water (*k*₄). For the latter, although this is not kinetically differentiated in the model, basic heterocyclic boronic acids can engage in a pre-equilibrium (*K*₄) with autoionized water to generate a zwitterionic adduct (X_{ZW}). For the boronate form (X_{OH}), there are the base-catalyzed Kuivila process (*k*₂), concentration-dependent autocatalysis (*k*_{2cat}) occurring with rate maximum when pH = pK_a, and the Perrin mechanism involving base-catalyzed protonolysis (*k*₃). For the latter, although this is not kinetically differentiated in the model, the boronate can engage with hydroxide in a pre-equilibrium (*K*₃) to generate the dianion (X_O). Finally, for the N-protonated form (X_{H+}), this being distinct from the zwitterion (X_{ZW}) due to the presence of a boronic acid, not a boronate, there is a direct protodeboronation by water (*k*₅).

As indicated graphically beside the protodeboronation mechanisms in the model (Figure 5), each of the six processes (*k*₁, *k*₂, *k*_{2cat}, *k*₃, *k*₄, *k*₅) has a distinct pH-log *k*_{obs} profile. It can be instructive to consider hypothetical combinations of selected pH-log *k*_{obs} relationships; examples (i, ii, and iii) are

preconfigured in the spreadsheet provided in the SI. By mathematical combination of all six steps (see SI for full derivation) and calculation of the three-state speciation, an “overall rate equation” (Figure 5, center) can be generated. The equation allows analysis of the empirical rate (k_{obs}) as a function of pH and boronic acid concentration, using up to nine constants: pK_a , pK_{aH} , k_1 , k'_2 , $k'_2\text{cat}$, k'_3 , k'_4 , k'_5 , pK_w in which processes indicated by the term k' contain amalgamated constants (e.g., K , k , and $[\text{H}_2\text{O}]$). For nonbasic boronic acids, pK_{aH} is nominally set to -5 to preclude X_{H^+} speciation.

Values for pK_a and pK_{aH} can be determined independently, or via the pH–log k_{obs} simulation. Initial pK_{aH} values for 6–17 were determined by ^1H NMR pH titration (1:1 $\text{H}_2\text{O}/1,4$ -dioxane, 25 °C), Table 2. An empirical correction for temperature (ΔpK_{aH} 25–70 °C = -0.46) was determined from the pH–rate profile simulation. Generally, the $\text{B}(\text{OH})_2$ unit slightly decreases the basicity relative to the parent heterocycle.³⁴ For example, 2-, 3-, and 4- pyridyl boronic acids (15, 9, 10) have pK_{aH} values (25 °C) of 3.86, 4.22, and 3.82, compared to that of 4.38 for pyridine, see SI. The pK_a values for most of the boronic acids were measured by ^{11}B NMR pH titration (1:1 $\text{H}_2\text{O}/1,4$ -dioxane, 70 °C); the pK_a of the more reactive species (5, 12, 15–17) were estimated via the pH–log k_{obs} simulation.

5. pH–Rate Profiles Analysis of Boronic Acids 2–19. Using the rate equation in Figure 5, the pH–rate profiles for 2–19 were simulated by automated iteration of rate and equilibrium constants, minimizing the sum square error (SSE) between predicted and observed data across the full profile (pH 1–13). The SSE-minimized fitting constants are provided in Table 2. In all cases (2–19), only a subset of the six pathways (k_1 , k'_2 , $k_2\text{cat}$, k'_3 , k'_4 , k'_5) were required for satisfactory simulation (solid lines through data, Figure 4). The constants that are not required for simulation, but are in principle feasible, are reported as threshold values (\leq) that induce a $\leq 5\%$ change in the SSE.³⁵

Nonbasic Heterocycles (2–5). The thienyl (2, 3) and furyl (4) boronic acids (Figure 4, profile I) required only the Kuivila processes (k_1 , k'_2)^{17c,k} and autocatalysis ($k_2\text{cat}$) for simulation. The 2-pyrrolyl boronic acid 5 required an additional pH-independent process (k'_4)²¹ to fit the data between pH 3 and 6. This process is slow enough (k'_4 , half-life > 24 days) to be consistent with a water autoionization mechanism.³⁶ Higher reactivity of 2- versus 3-thienyl and furyl boronic acids has been noted before, but only for acid-catalysis (k_1).²² In all cases (2–5), the base-catalyzed process (k'_2) is more efficient than the acid (k_1), and the rates rise substantially through the series; above pH 11, 2-pyrrolyl 5 has a half-life of less than 3 min.

Basic Heterocycles (6–17). The rate data obtained for 2-pyridyl boronic acids 15–17 (profile II) show a near inverse pH–rate profile compared to that of the nonbasic heterocycles 2–5 (profile I) and required just a single term (k'_4) for simulation. Maximum rates are attained when speciation disfavors the boronate ($15\text{--}17_{\text{OH}}$; high pH) and pyridinium ($15\text{--}17_{\text{H}^+}$; low pH) forms. Thus, for the least basic 17 ($pK_{\text{aH}} < -0.6$), the protodeboronation is not detectably attenuated by acid, even at pH 1. The much less reactive 5-pyrimidyl (8) and 3-pyridyl (9) systems required base-catalysis ($k'_2 + k_2\text{cat}$) in addition to the neutral mechanism (k'_4) for simulation. The 5-pyrazolyl and 5-thiazolyl boronic acids (13–15) were highly reactive, requiring both k'_4 (neutral) and k'_2 (basic) pathways for satisfactory simulation, with rates attenuated at pH below their pK_{aH} (profile III). The 4-pyridyls (10, 11) are of similar

reactivity to 3-pyridyl (9), but differ in that they still protodeboronate effectively at a pH substantially below their pK_{aH} (profile III). This effect was satisfactorily simulated by including a direct (H_2O -mediated) protodeboronation of the conjugate acid (k'_5); the 4-pyridyl systems (10, 11) were the only species requiring this. The two remaining basic heterocycles, 4-pyrazolyl (6) and 4-isoxazolyl (7), gave the most complex profiles, requiring acid (k_1), base ($k'_2/k_2\text{cat}$), base-catalyzed boronate (k'_3), and neutral (k'_4) pathways (profile IV; Figure 4). These were the only examples requiring the Perrin mechanism (k'_3), a process that in $\text{Ar}\text{--}\text{B}(\text{OH})_2$ systems is proposed to require 2,6-disubstitution.^{17k}

Vinyl and Cyclopropyl Boronic Acids (18–19). Strongly acidic or basic solutions were required to effect any significant protodeboronation of the vinyl (18) and cyclopropyl (19) boronic acids (profile IV). Even at pH ≥ 11 , the half-lives are weeks. A small selection of simple alkyl boronic acids (Me, *c*-Bu, and *c*-Hex) were also investigated. The extremely slow reactions (half-lives of months, see SI) made it difficult to clarify, by $^1\text{H}/^{13}\text{C}/^{11}\text{B}$ NMR analysis, if protodeboronation was the major pathway of decomposition, rather than, for example, oxidation.

6. Protodeboronation Mechanisms for Basic Heterocycles. To aid rationalization of the diverse range of pH profiles for basic heterocycles 6–17, protodeboronation mechanisms were explored by ^{11}B NMR, DFT calculations (M06L/6-311++G**;²³ see SI for details), and by testing the effect of additives.

Zwitterionic Water Adducts (X_{ZW}). 2-Pyridyl boronic acids are notorious for their susceptibility to protodeboronation,^{1,8,11–13} as is found for 15–17. However, only a single neutral process (k'_4) is required for simulation of the full pH–rate profile, indicating that the classic Kuivila-type acid- and base-catalyzed mechanisms (k_1 and k'_2) are negligible processes. Indeed H^+/OH^- act as powerful protodeboronation inhibitors by modulating the speciation: the proportion of neutral boronic acid available for reaction by k'_4 is reduced by conversion to the protonated ($15\text{--}17_{\text{H}^+}$) or boronate ($15\text{--}17_{\text{OH}}$) forms. Consequently, 2-pyridyl boronic acid 15 shows surprising stability at high pH (profile II, Figure 4) undergoing protodeboronation as slow, or slower, than many of the other heterocycles tested (e.g., 3–7, 12–14). The protodeboronation of 15–17 by water (k'_4) has a much lower energy barrier than the analogous protonation (k_2) of the boronate ($15\text{--}17_{\text{OH}}$). Irrespective of the likely contribution to direct hydrolysis by dynamic water fluctuation,³⁶ the free energy barriers calculated (DFT) for concerted aqueous cleavage of the C–B bond in neutral species 15–17 (47.9, 46.3, and 46.9 kcal/mol respectively) are far too high to account for the observed rates.

The ^{11}B NMR spectra of pyridyl species 15–17 in the pH region where maximum rate is attained (pH 4–8, profile II, Figure 4) each display a *single* peak, arising from rapid equilibrium of the neutral boronic acid ($15\text{--}17$, approximately 28 ppm, broad) with a zwitterionic boronate $15\text{--}17_{\text{ZW}}$ (approximately 1 ppm, sharp). The zwitterionic species is formally generated by amphoteric capture of autoionized water (H^+ , OH^-) at the Bronsted-basic and Lewis-acidic (N, B) centers. At pH 6.5, the time-average chemical shifts, Figure 6, show that the equilibrium position between $15\text{--}17$ and $15\text{--}17_{\text{ZW}}$ (K_4) is strongly modulated by the electron demand of the 6-substituent.

A key feature in all of the protodeboronations proceeding via fragmentation of zwitterionic water adducts (k_4) is the

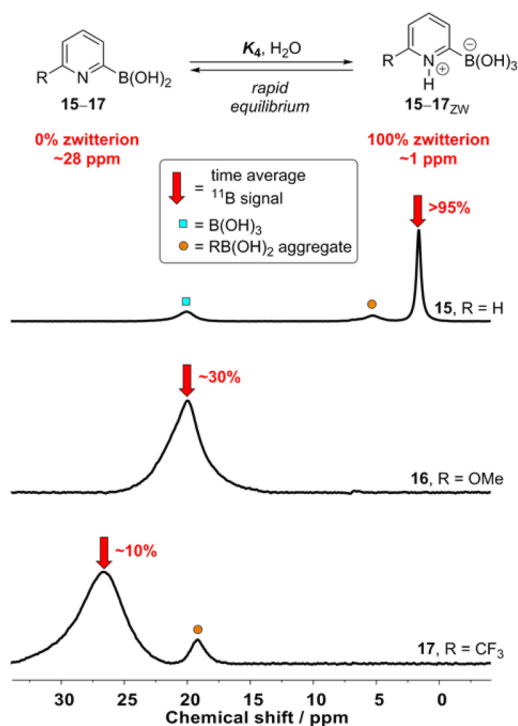


Figure 6. ^{11}B NMR spectra of 2-pyridyl boronic acids **15–17** (0.01 M, 25 °C) at pH 6.5 (AcO[−]/AcOH buffer). Peaks correspond to time-average weighted chemical shifts between **15–17** (28 ppm, broad) and **15–17**_{ZW} (1 ppm, sharp). Additional minor species are B(OH)₃ and aggregates, (RB(OH)₂)_n, as indicated.

intramolecular stabilization of the B(OH)₃ leaving group as C–B cleavage occurs. For the 2-pyridyl systems (e.g., TS **15**_{ZW}, k_4 , Figure 7) this involves hydrogen bonding with the positively charged pyridinium NH; in effect this solvates the B(OH)₃. However, this high reactivity (k_4) is not restricted to species with a protonated basic nitrogen atom adjacent to boron. Thiazolyl and pyrazolyl boronic acids (**12–14**), where the basic site is remote from boron, and for which water autoionization equilibria with zwitterionic species (**12–14**_{ZW}) is not detected (<10%) by ^{11}B NMR, also undergo rapid protodeboronation. DFT calculations support this observation: generation of the zwitterions (**12–14**_{ZW}) is much less favorable than for the pyridyl isomers **14–16**_{ZW}, but the transition states for their fragmentation (TS **12–14**_{ZW}, k_4 , Figure 7) are comparable in energy, due to other stabilizing interactions with the B(OH)₃ leaving group. For the thiazolium boronate (**12**_{ZW}, k_4), the antibonding orbital (C–S σ^*) acts as a surrogate H-bond, an extreme example of the interaction recently discussed by Meanwell.³⁷ For the pyrazolium systems (**13**, **14**), the highly polarized CH bond of the *N*-methyl (**13**_{ZW}, k_4) and NH (**14**_{ZW}, k_4) adjacent to NH⁺ play the same stabilizing roles during heteroaryl-B(OH)₃ zwitterion fragmentation.

In the high pH region (pH > pK_a; 8.5–9.1) where the zwitterions (**12–14**_{ZW}) are converted to boronates (**12–14**_{OH}), the stabilizing interactions provided by C–S σ^* , CH, and NH interactions are still active, albeit attenuated (neutral basic N rather than NH⁺). This attenuation is offset by the dominant boronate speciation, leading to only a small net reduction in protodeboronation rate (profile III, Figure 4). In contrast, for the pyridyl systems (**15–17**), the respeciation to boronates **15–17**_{OH} at high pH results in loss of the pyridinium NH

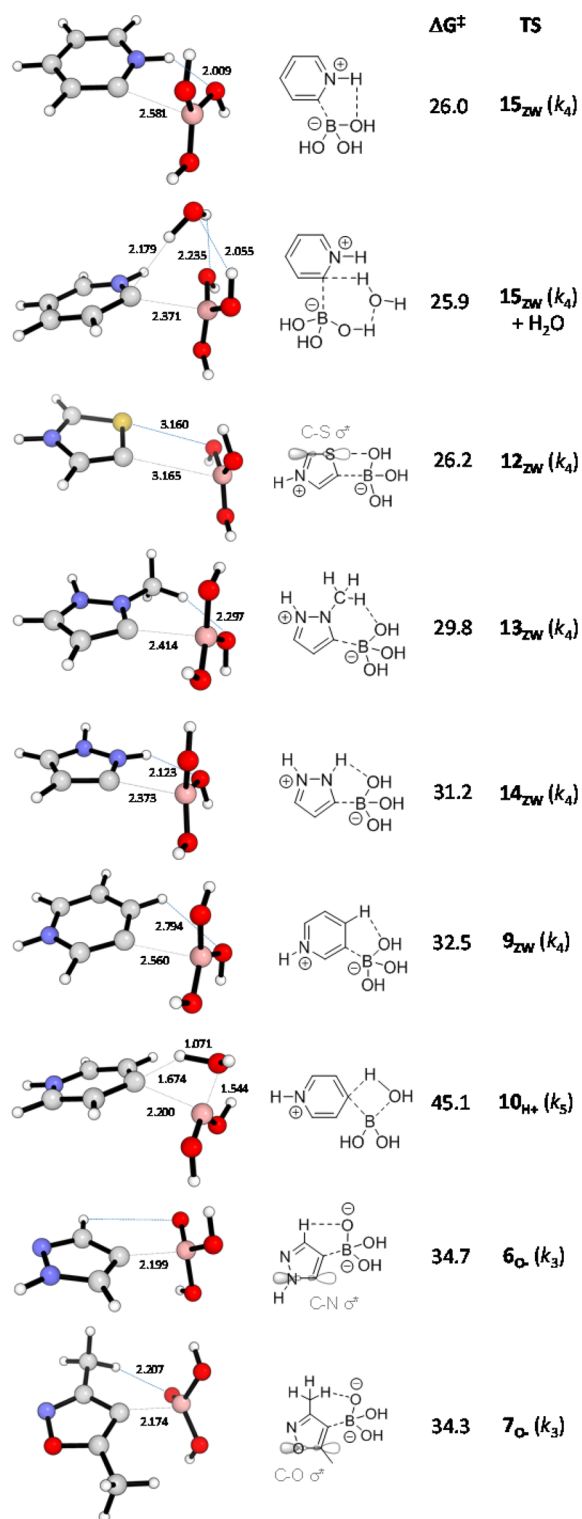


Figure 7. Selected transition state (TS) structures and calculated free energies (kcal/mol; M06L/6-311+G**)^{23–27} for pathways k_4 , k_5 , and k_3 , involving zwitterionic water adducts (**9**_{ZW}, **12**_{ZW}, **13**_{ZW}, **14**_{ZW}, **15**_{ZW}), pyridinium boronic acid (**10**_{H+}), and boronate dianions (**6**_{O-} and **7**_{O-}), respectively.

stabilizing interaction, and a markedly different behavior: the rate is strongly attenuated (profile II).

Equilibrium zwitterion populations are also low (^{11}B NMR; <10%) for 5-pyrimidyl (**8**), 3-pyridyl (**9**), and 4-pyridyl (**10**, **11**) boronic acids in neutral solution. This contrasts earlier

reports where 3- and 4-pyridinium boronate zwitterions (9_{ZW} and 10_{ZW}) were concluded to be dominant (>90%) on the basis of UV analysis of **9** and **10** in pure aqueous solution.^{8d} DFT calculations suggest that not only are 3-pyridyl 9_{ZW} and 4-pyridyl 10_{ZW} higher in energy than 2-pyridyl 15_{ZW} , but also that the greater charge separation, lack of ylidic character,³⁸ and poorer stabilization of the departing $B(OH)_3$ in the fragmentation (k_4) reduce their reactivity compared to **15**–**17**. The approximately 6 kcal/mol higher barriers for fragmentation near-quantitatively predict the 4 orders of magnitude slower reaction, e.g., compare 3-pyridyl- 9_{ZW} , k_4 , with 2-pyridyl- 15_{ZW} , k_4 , Figure 7.

Protodeboronation at 4-Pyridinium (k_5). Despite 3-pyridyl (**9**) and 4-pyridyl (**10**) boronic acids undergoing protodeboronation via zwitterionic intermediates (9_{ZW} and 10_{ZW}) at similar rates, there is a key difference between their pH–rate profiles (see profiles II and III, Figure 4). For the 3-pyridyl system (**9**) the rate is strongly attenuated when the pH approaches and goes below pK_{aH} (3.60) due to respeciation of the neutral $9/9_{ZW}$ form to 9_{H+} , where the N is fully protonated and the B-center is boronic acid, not boronate. In contrast, the 4-pyridyl boronic acids (**10**, **11**) display near-constant k_{obs} as the pH migrates through and below the pK_{aH} (3.36 and 2.95) indicative that the pyridinium species (10_{H+} , 11_{H+}) are also reactive components. A mechanism involving attack at the boron in pyridinium 10_{H+} by water to access a dipolar carbene^{38,39} intermediate is supported by DFT studies, Figure 7. The barrier for this process ($10_{H+}/k_5$; Figure 7), while high, is close to that computed for the normal protodeboronation under neutral conditions.

Boronate Deprotonation (k'_3). As noted above, k'_3 , a mechanism in which base catalyzes the decomposition of the boronate, was required for kinetic simulation of 4-pyrazolyl (**6**) and 4-isoxazolyl (**7**) boronic acids at high pH. The Perrin mechanism (k'_3) has previously only been found in aryl systems bearing 2,6-disubstitution.^{17k,39} The data, obtained at pH 12–13 (profile IV, Figure 4), the upper limit of the pH range attainable while retaining homogeneous reactions, confirm the first-order dependence on $[OH^-]$ and on boronate ($6_{OH}/7_{OH}$), i.e., an increase (gradient +1.0) of $\log k_{obs}$ with pH, after the k_2 -plateau. In principle, if boronate deprotonation is at equilibrium, a second pH rate plateau will be reached (at much higher pH than explored) after boronates $6_{OH}/7_{OH}$ are fully converted to $6_{O-}/7_{O-}$.

DFT calculations²³ suggest that protodeboronation via k'_3 requires the heterocycle to be able to stabilize both the deprotonated boronate ($6_{O-}/7_{O-}$) and the carbanion arising from its C–B fragmentation (k_3). The 4-pyrazolyl ring (TS 6_{O-} , k_3 ; Figure 7) facilitates this stabilization using the adjacent C–N σ^* orbital; an analogous C–O σ^* orbital is available with the 3-isoxazolyl ring (TS 7_{O-} , k_3 ; Figure 7) (**6**). In contrast, although a 5-pyrazolyl ring (14_{O-}) can stabilize the boronate by interaction with the adjacent NH, it cannot provide stabilization of a carbanion arising by C–B fragmentation. As a consequence, at high pH the protodeboronation rates of **6** and **7**, but not **14**, rise as the concentration of $[OH^-]$ becomes sufficient to deprotonate the corresponding boronates.

Bis-boronate Protolysis (k'_2 -mono and k'_2 -bis). Prompted by the problems caused by protodeboronation when bis-boryl species are employed in copolymerization cross-couplings under basic conditions,⁴⁰ we also determined the protodeboronation kinetics of a bis-boronic acid. The rates provide information on the intramolecular effect of one boronic acid

on the reactivity of another. Choosing a simple 2,5-thienyl substrate, **20**, we simulated the kinetics using a model (Figure 8) in which there are two aqueous association constants (K_a -

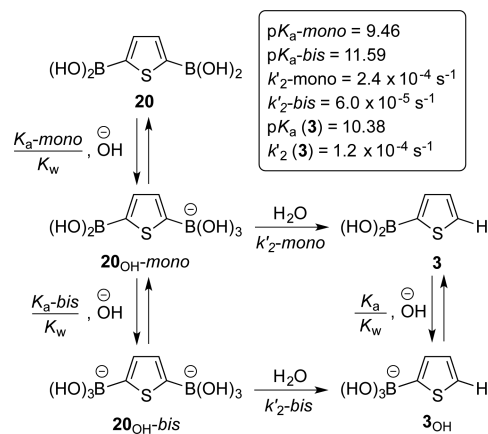


Figure 8. Rate comparison of protodeboronation of 2,5-bis-boronyl thiophene **20** and 2-boronyl thiophene **3** in the range pH 6–13 (50 mM, 1:1 dioxane/ H_2O , 70 °C); rate and equilibrium constants obtained by pH–rate profile simulation, pH 6–13, see SI.

mono and K_a -bis) and two protonolysis rates (k'_2 -mono and k'_2 -bis) for the resulting boronates (20_{OH} -mono and 20_{OH} -bis). From this data, it can be seen that 20_{OH} -mono reacts 2-fold faster than the 2-thienyl-boronate 3_{OH} ; in other words, the presence of the spectator boronic acid in 20_{OH} -mono has a small impact on the rate, and slightly increases the Lewis acidity at boron ($pK_a = 9.5$). In contrast, 20_{OH} -bis is about 8-fold less reactive than 20_{OH} -mono, when statistically normalized, indicating that the boronate group induces mild rate suppression, and substantially decreases the Lewis acidity at boron ($pK_a = 11.6$). As such, using media at a higher than usual pH may be of benefit in polymerization cross-couplings of bis-boryl species.

7. Effect of Additives (Cu, Zn, B) on Protodeboronation. In addition to identification of the zwitterionic water adduct (15_{ZW}) of 2-pyridyl boronic acid by ^{11}B NMR, analysis at various concentrations revealed the presence of aggregates, $(15)_n$ ($\delta_B \approx 6$ ppm, see Figure 6). Analysis of the protodeboronation kinetics at various concentrations revealed that generation of aggregates reduces the proportion of zwitterion generated, resulting in mildly attenuated protodeboronation rates; compare entries A and B, Table 3. The pseudo-first-order kinetics obtained in these protodeboronation reactions indicate that the boric acid co-product also attenuates protodeboronation, as confirmed by reaction of **15**, 0.05 M, in the presence of added boric acid, 0.15 M, entry C. Other Lewis acid additives ($MgCl_2$, $Sc(OTf)_3$, $ZnCl_2$, and $CuCl_2$; entries D–G) were tested, of which $CuCl_2$, the most azaphilic, had the greatest impact, increasing the half-life of **15** by a factor of 24.

Analysis of this process (entry G) *in situ* by NMR was not informative due to the paramagnetic $Cu(II)$. However, addition of 2,2'-bipyridine during a $CuCl_2$ -attenuated protodeboronation (entry H, Figure 9) resulted in reinstatement of rapid protodeboronation, through competition of **15** and 2,2'-bipyridine for the Cu. Thus, irreversible transmetalation (Cu for B) is not responsible for the protodeboronation rate suppression.

^{11}B NMR analysis of the reaction of **15** containing a $ZnCl_2$ additive^{13c} (entry F) indicated that a boronate is still present

Table 3. Effect of Additives on the Protodeboronation Kinetics of 12–15 at pH 6.2–6.9 in 1:1 H₂O/1,4-Dioxane at 70 °C

| entry | [RB(OH) ₂] | additive (conc) | <i>k</i> _{obs} 10 ³ /s ⁻¹ | <i>t</i> _{1/2} |
|-------|------------------------|---|--|-------------------------|
| A | 15, 0.05 M | | 27.9 | 25 s |
| B | 15, 0.20 M | | 20.8 | 33 s |
| C | 15, 0.05 M | B(OH) ₃ (0.15 M) | 20.0 | 34 s |
| D | 15, 0.05 M | MgCl ₂ (0.10 M) | 28.8 | 24 s |
| E | 15, 0.05 M | Sc(OTf) ₃ (0.10 M) | 12.9 | 53 s |
| F | 15, 0.05 M | ZnCl ₂ (0.10 M) | 8.4 | 82 s |
| G | 15, 0.05 M | CuCl ₂ (0.10 M) | 1.20 | 10 min |
| H | 15, 0.05 M | CuCl ₂ (0.10 M) ^a | 16.9 | 41 s ^a |
| I | 12, 0.05 M | | 14.4 | 48 s |
| J | 12, 0.05 M | ZnCl ₂ (0.10 M) | 50.5 | 14 s |
| K | 13, 0.05 M | | 0.184 | 63 min |
| L | 13, 0.05 M | ZnCl ₂ (0.10 M) | 2.20 | 5 min |
| M | 14, 0.05 M | | 0.068 | 169 min |
| N | 14, 0.05 M | ZnCl ₂ (0.10 M) | 0.902 | 13 min |

^aBipy (0.2 M) added at 80 s.

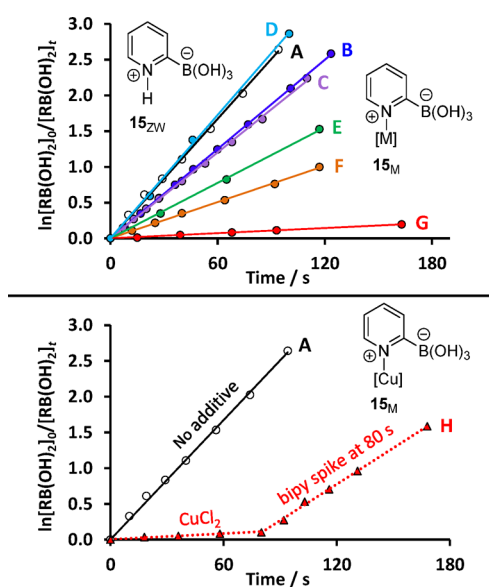


Figure 9. Pseudo-first-order protodeboronation kinetics for 15 in the presence of Lewis acid additives.

(δ_B 1.5 ppm). The inhibiting effect thus arises from reversible pyridine complexation (15_M ; $M = \text{Zn, Cu, etc.}$), reducing the proportion of zwitterion (15_{ZW}) available for fragmentation (k_4). As noted above, the 5-thiazolium system undergoes rapid protodeboronation (12_{OH} k'_4 ; and 12_{ZW} k'_4 ; Figure 7) through C–S σ^* stabilization of the TS for fragmentation. Thus, unlike the 2-pyridyl system 15, which relies on stabilization by the adjacent NH⁺, metal complexation at the 5-thiazolium nitrogen (12_M) does not negate the stabilization, but in contrast exacerbates the effect of the C–S σ^* , resulting in even faster protodeboronation (entries I and J, Figure 10). The same effects are found for 13 and 14, where N-complexation by [Zn] augments the boronate stabilizing effect of the N-methyl (13_M) and NH (14_M) groups, resulting in more rapid protodeboronation (Table 3, entries K–N, Figure 10).

CONCLUSIONS

As summarized in Figure 11, and contrary to general perception, many heterocyclic systems, including 2–5 and 8–

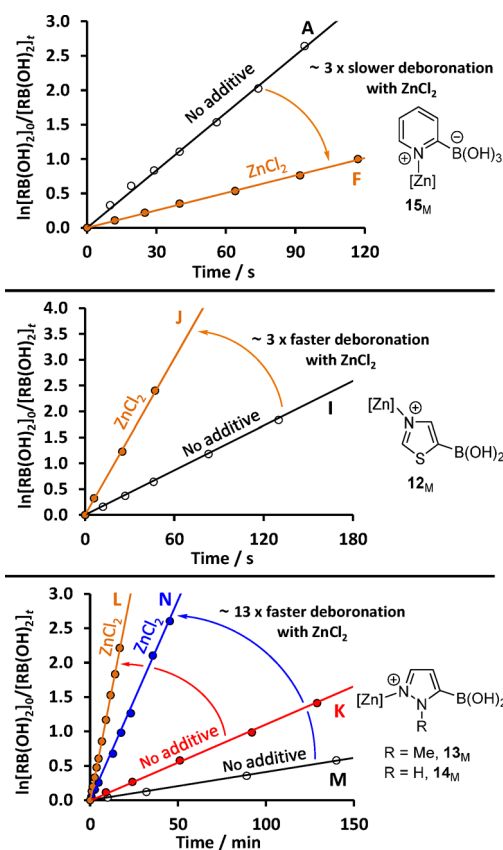


Figure 10. Effect of 2 equiv of ZnCl₂ on protodeboronation of 12–15 in 1:1 H₂O/1,4-dioxane, 70 °C, pH 6.2–6.9 (NaOAc/AcOH).

11, undergo very slow aqueous protodeboronation, even at very high pH. Large stoichiometric excess can often be required for the successful Suzuki–Miyaura coupling of vinyl (18) and cyclopropyl (19) boronic acids. The resistance of 18 and 19 to protodeboronation (half-lives of weeks) suggests that cross-coupling conditions,¹⁹ rather than intrinsic reagent instability, cause this. Nonetheless, some heterocyclic boronic acids, e.g., 6, 7, 12–17, can undergo rapid protodeboronation, but only in specific pH ranges. In all of these cases rapid protodeboronation is facilitated by stabilization of the B(OH)₃ during C–B fragmentation. For the 2-pyridyl system, this stabilization is provided by the pyridinium NH in a zwitterion (15 – 17_{ZW}); in 12, it is provided by an adjacent C–S σ^* , and in 13, 14 by an adjacent polarized NMe or NH. Additional stabilization of the carbanion arising from C–B fragmentation (k_3) is provided in 5-pyrazolyl and 5-isoxazolyl systems by adjacent C–N σ^* (6) and C–O σ^* (7) orbitals. N-Alkylation, e.g., to generate methylpyridinium boronates,⁴¹ will reduce p*K*_a, making k_2 accessible at a lower pH. N-Methylation may also effect stabilization of B(OH)₃ during 2-pyridyl C–B fragmentation by interaction with the highly polarized N–CH₃ unit, analogous to that in 13_{ZW} , k_4 , Figure 7.

A key aspect in all of the reactive systems studied (6, 7, 12–17) is that the pH controls the speciation of the boronic acid (X) between various protonated, neutral, boronate, and deprotonated states (X_{H^+} , X_{ZW} , X, X_{OH} , and X_{O^-}). The speciation regulates which specific protodeboronation processes (k_1 , k_2 , k_{2cat} , k_3 , k_4 , k_5) are available, and thus governs the overall rate.

For example, 2-pyridyl-boronic acid (15) has a half-life of ≥ 2 h at pH 1 (as 15_{H^+}) or at pH 13 (as 15_{OH}) but just 26 s

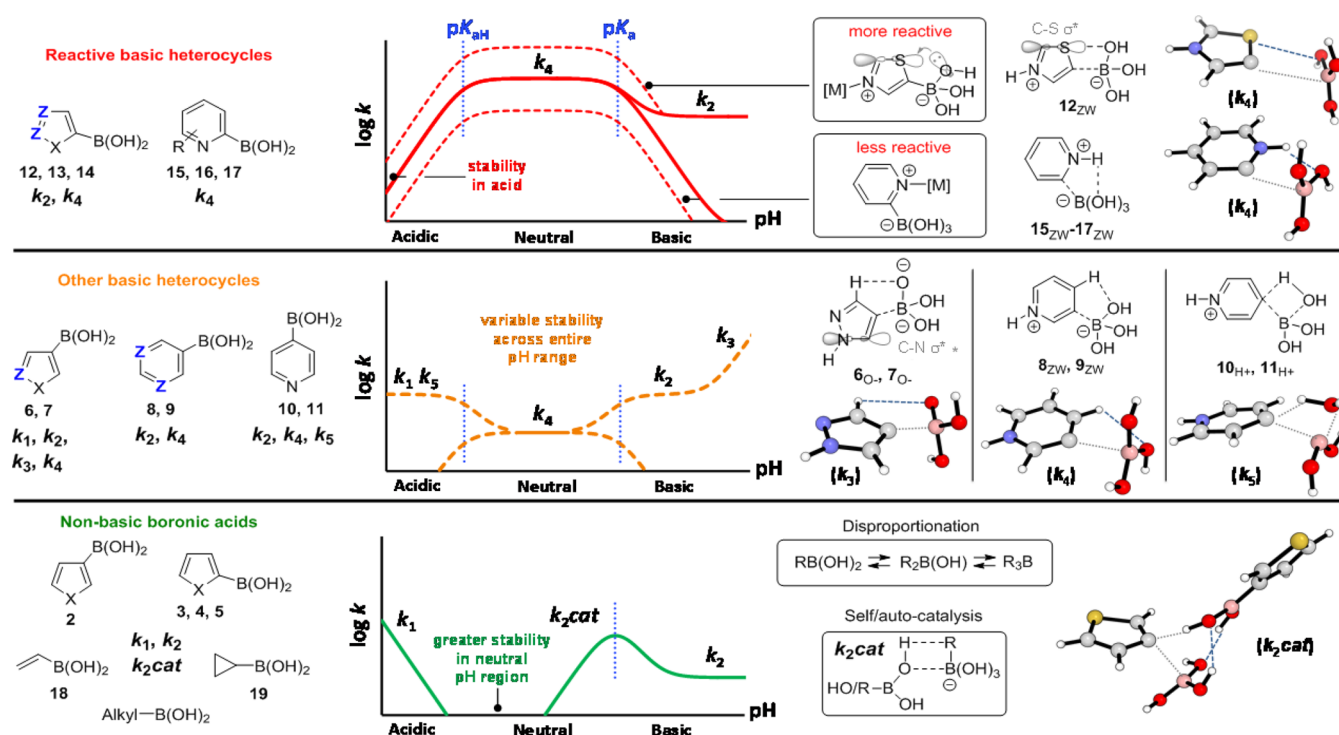


Figure 11. Schematic relationships for protodeboronation rate ($\log k_{\text{obs}}$) and pH (arbitrary scale, refer to I–IV, Figure 4) allowing classification of boronic acids according to the impact of basic sites ($Z = \text{N}_{\text{Ar}}$), antibonding orbitals, and effect of added Lewis acids (MX_n). In structures where more than one Z is indicated, only one site needs to be basic (i.e., N_{Ar}); the remainder can also be CH, CR, CX, etc.

between pH 4 and 10 because maximum 15_{ZW} is available for pathway k_4 . Electron withdrawing groups in the 6-position (16, 17) reduce both $\text{p}K_{\text{aH}}$ and $\text{p}K_{\text{a}}$, resulting in the high reactivity being expressed in a lower pH range. In contrast to 2-pyridyl-15, 5-thiazolyl and 5-pyrazolyl boronic acids are reactive in both the zwitterionic ($12\text{--}14_{\text{ZW}}$, k_4) and boronate ($12\text{--}14_{\text{OH}}$, k_2) forms, leading to a much wider pH range for fast protodeboronation (compare profiles II and III, Figure 4).

When high concentrations of boronic acid and boronate are present, bimolecular processes can occur, resulting in protodeboronation autocatalysis ($k_{2\text{cat}}$, Figures 1 and 2) and disproportionation (Figure 3). While borinic ($\text{R}_2\text{B}(\text{OH})$) and borane (R_3B) reagents have been employed in Suzuki–Miyaura couplings,⁴² their different reactivity may lead to more complex reaction profiles. The slow release^{9a,11a} of boronic acids from MIDA boronates,^{8a,9a,15} or trifluoroborates,¹⁶ maintains low $\text{RB}(\text{OH})_2$ concentrations, and can thus reduce competing bimolecular autocatalysis and disproportionation. This will be most important in the range $\text{pH} = \text{p}K_{\text{a}} \pm 1.6$, where the speciation allows coexistence⁴³ of boronic acid and boronate.

Lewis acid additives (Table 3, Figures 9 and 10) can exacerbate or attenuate protodeboronation of basic heterocycles, across the whole pH range. For the 2-pyridyl systems, protodeboronation rates are reduced by lowering the zwitterion concentration ($15\text{--}17_{\text{ZW}}$, k_4). This may partially explain the beneficial effect of additives, such as copper salts, in the coupling of 2-pyridyl boronic acids.^{8c,13} However, Lewis acids have the opposite effect for $12\text{--}14$, where complexation to the remote basic nitrogen augments boronate stabilization (by $\text{C}\text{--}\text{S}\sigma^*$, NMe, and NH) at the fragmentation TS (k_2/k_3) thus accelerating protodeboronation.

Our kinetic studies (Tables 1 and 2) also provide insight into other protodeboronation reactions. For example, Perrin found *p*-anisyl boronic acid (1) to equilibrate instantly with the

corresponding trifluoroborate (ArBF_3K) in aqueous HCl/KHF_2 (pH 2), with protodeboronation to generate 1_{H} occurring with a half-life of less than 3 min. At pH 2, the half-life of 1 is 11 h at 90 °C (k_1 , Table 1, entry 1). Clearly the protodeboronation proceeds *directly* from the trifluoroborate, as was suggested by Perrin.^{17k} In contrast to 1, where the concentration of the trihydroxyboronate form (1_{OH}) is vanishingly low at low pH, the trifluoroborate form ArBF_3K is stable under these conditions (pH 2), and $\text{C}\text{--}\text{B}$ protonolysis (k_2 , H^+) is anticipated to be fast. On this basis, 2-pyridyl trifluoroborates are also expected to readily protodeboronate, as reported by Molander.⁴⁴

In summary, heteroaromatic boronic acids 2–17 undergo protodeboronation in 1:1 dioxane/ H_2O at 70 °C with a diverse range of rates and pH profiles (Figures 2 and 4). While there is no overall trend in terms of reactivity or specific pH zones for highest stability, each class of heteroaromatic boronic acid (Figure 11) can be evaluated for likely speciation at a given pH, and factors that induce instability identified. These factors include (i) a basic nitrogen center that allows zwitterion generation by reaction with autoionized water; (ii) an $\text{N}\text{--}\text{H}$, $\text{X}\text{--}\text{H}$, or polarized $\text{NC}\text{--}\text{H}$ group adjacent to the boronate to interact and stabilize it during $\text{C}\text{--}\text{B}$ fragmentation; and (iii) an adjacent antibonding orbital ($\text{C}\text{--}\text{X}\sigma^*$, $\text{X} = \text{S}, \text{N}, \text{O}$) that can overlap with the carbanion formally generated during $\text{C}\text{--}\text{B}$ fragmentation.

■ ASSOCIATED CONTENT

Supporting Information

The Supporting Information is available free of charge on the ACS Publications website at DOI: 10.1021/jacs.6b03283.

Spreadsheet to assist with model application (XLSX)

Kinetic data, simulation, synthesis, characterization, and NMR spectra (PDF)

AUTHOR INFORMATION

Corresponding Author

*Guy.lloyd-jones@ed.ac.uk

Notes

The authors declare no competing financial interest.

ACKNOWLEDGMENTS

We thank Craig P. Butts, Juraj Bella, and Lorna Murray for NMR assistance. A.G.L. thanks the NSCCS for computational support and Gary Noonan for useful discussions. The research leading to these results has received funding from the European Research Council under the European Union's Seventh Framework Programme (FP7/2007–2013)/ERC grant agreement 340163.

REFERENCES

- (1) *Boronic Acids: Preparation and Applications in Organic Synthesis, Medicine and Materials*, 2nd ed.; Hall, D., Ed; Wiley VCH: Weinheim, Germany, 2011; Vols. 1 and 2, pp 1–133.
- (2) (a) Miyaura, N.; Yamada, K.; Suzuki, A. *Tetrahedron Lett.* **1979**, *20*, 3437–3440. (b) Miyaura, N.; Suzuki, A. *Chem. Rev.* **1995**, *95*, 2457–2483.
- (3) Cho, C. S.; Uemura, S. *J. Organomet. Chem.* **1994**, *465*, 85–92.
- (4) (a) Chan, D. M. T.; Monaco, K. L.; Wang, R.-P. P.; Winters, M. P. *Tetrahedron Lett.* **1998**, *39*, 2933–2936. (b) Evans, D. A.; Katz, J. L.; West, T. R. *Tetrahedron Lett.* **1998**, *39*, 2937–2940. (c) Lam, P. Y. S.; Clark, C. G.; Saubern, S.; Adams, J.; Winters, M. P.; Chan, D. M. T.; Combs, A. *Tetrahedron Lett.* **1998**, *39*, 2941–2944.
- (5) Liebeskind, L. S.; Srogl, J. *J. Am. Chem. Soc.* **2000**, *122*, 11260–11261.
- (6) (a) Sakai, M.; Hayashi, H.; Miyaura, N. *Organometallics* **1997**, *16*, 4229–4231. (b) Cho, C. S.; Motofusa, S.; Ohe, K.; Uemura, S.; Shim, S. C. *J. Org. Chem.* **1995**, *60*, 883–888.
- (7) (a) Sakai, M.; Ueda, M.; Miyaura, N. *Angew. Chem., Int. Ed.* **1998**, *37*, 3279–3281. (b) Takezawa, A.; Yamaguchi, K.; Ohmura, T.; Yamamoto, Y.; Miyaura, N. *Synlett* **2002**, *10*, 1733–1735.
- (8) (a) Review: Tyrrell, E.; Brookes, P. *Synthesis* **2003**, *2003*, 469–483. (b) Ishiyama, T.; Ishida, K.; Miyaura, N. *Tetrahedron* **2001**, *57*, 9813–9816. (c) Dick, G. R.; Woerly, E. M.; Burke, M. D. *Angew. Chem., Int. Ed.* **2012**, *51*, 2667–2672. (d) Fischer, F. C.; Havinga, E. *Recl. des Trav. Chim. des Pays-Bas* **1974**, *93*, 21.
- (9) (a) Knapp, D. M.; Gillis, E. P.; Burke, M. D. *J. Am. Chem. Soc.* **2009**, *131*, 6961–6963. (b) Matteson, D. S. *J. Am. Chem. Soc.* **1960**, *82*, 4228. (c) Peyroux, E.; Berthiol, F.; Doucet, H.; Santelli, M. *Eur. J. Org. Chem.* **2004**, *2004*, 1075–1082. (d) Denmark, S. E.; Butler, C. R. *Chem. Commun.* **2009**, *1*, 20–33.
- (10) (a) Molander, G. A.; Gormisky, P. E. *J. Org. Chem.* **2008**, *73*, 7481–7485. (b) Lemhadri, M.; Doucet, H.; Santelli, M. *Synth. Commun.* **2006**, *36*, 121–128. (c) Wallace, D. J.; Chen, C. *Tetrahedron Lett.* **2002**, *43*, 6987–6990. (d) Zhou, S.-M.; Deng, M.-Z.; Xia, L.-J.; Tang, M.-H. *Angew. Chem., Int. Ed.* **1998**, *37*, 2845–2847. (e) Chen, X.; Goodhue, C. E.; Yu, J. Q. *J. Am. Chem. Soc.* **2006**, *128*, 12634–12635. (f) Chen, H.; Deng, M.-Z. *Org. Lett.* **2000**, *2*, 1649–1651. (g) Fang, G. H.; Yan, Z. J.; Deng, M. Z. *Org. Lett.* **2004**, *6*, 357–360.
- (11) (a) Lennox, A. J. J.; Lloyd-Jones, G. C. *Isr. J. Chem.* **2010**, *50*, 664–674. (b) Lennox, A. J. J.; Lloyd-Jones, G. C. *Chem. Soc. Rev.* **2014**, *43*, 412–443.
- (12) Kinzel, T.; Zhang, Y.; Buchwald, S. L. *J. Am. Chem. Soc.* **2010**, *132*, 14073–14075.
- (13) (a) Deng, J. Z.; Paone, D. V.; Ginnetti, A. T.; Kurihara, H.; Dreher, S. D.; Weissman, S. A.; Stauffer, S. R.; Burgey, C. S. *Org. Lett.* **2009**, *11*, 345–347. (b) Chen, J.; Cammers-Goodwin, A. *Tetrahedron Lett.* **2003**, *44*, 1503–1506. (c) Chen, K.; Peterson, R.; Math, S. K.

LaMunyon, J. B.; Testa, C. A.; Cefalo, D. R. *Tetrahedron Lett.* **2012**, *53*, 4873–4876.

(14) Robbins, D. W.; Hartwig, J. F. *Org. Lett.* **2012**, *14*, 4266–4269. (15) Li, J.; Grillo, A. S.; Burke, M. D. *Acc. Chem. Res.* **2015**, *48*, 2297–2307.

(16) (a) Molander, G. A. *J. Org. Chem.* **2015**, *80*, 7837–7848. (b) Butters, M.; Harvey, J. N.; Jover, J.; Lennox, A. J. J.; Lloyd-Jones, G. C.; Murray, P. M. *Angew. Chem., Int. Ed.* **2010**, *49*, 5156–5160. (c) See ref 29 in: Lennox, A. J. J.; Lloyd-Jones, G. C. *J. Am. Chem. Soc.* **2012**, *134*, 7431–7441.

(17) (a) Ainley, A. D.; Challenger, F. *J. Chem. Soc.* **1930**, *52*, 2171–2180. (b) Johnson, J. R.; Van Campen, M. G.; Grummit, O. *J. Am. Chem. Soc.* **1938**, *60*, 111–115. (c) Kuivila, H. G.; Nahabedian, K. V. *J. Am. Chem. Soc.* **1961**, *83*, 2159–2163. (d) Kuivila, H. G.; Nahabedian, K. V. *J. Am. Chem. Soc.* **1961**, *83*, 2164–2166. (e) Nahabedian, K. V.; Kuivila, H. G. *J. Am. Chem. Soc.* **1961**, *83*, 2167–2174. (f) Kuivila, H. G.; Reuwer, J. F., Jr.; Mangravite, J. A. *Can. J. Chem.* **1963**, *41*, 3081–3090. (g) Kuivila, H. G.; Reuwer, J. F.; Mangravite, J. A. *J. Am. Chem. Soc.* **1964**, *86*, 2666–2670. (h) Beckett, M. A.; Gilmore, R. J.; Idrees, K. *J. Organomet. Chem.* **1993**, *455*, 47–49. (i) Frohn, H.-J.; Adonin, N. Y.; Bardin, V. V.; Starichenko, V. F. *Z. Anorg. Allg. Chem.* **2002**, *628*, 2834–2838. (j) Cammidge, A. N.; Crepy, K. V. *J. Org. Chem.* **2003**, *68*, 6832–6835. (k) Lozada, J.; Liu, Z.; Perrin, D. M. *J. Org. Chem.* **2014**, *79*, 5365–5368. (l) Noonan, G.; Leach, A. G. *Org. Biomol. Chem.* **2015**, *13*, 2555–2560.

(18) K_a is the equilibrium of RB(OH)_2 with $[\text{RB(OH)}_3]^-[\text{H}^+]$ and is distinct from K_{aH} , the N-protonation of basic heterocycles.

(19) See, e.g., (a) Kallepalli, V. A.; Gore, K. A.; Shi, F.; Sanchez, L.; Chotana, G. A.; Miller, S. L.; Maleczka, R. E., Jr.; Smith, M. R., III. *J. Org. Chem.* **2015**, *80*, 8341–8353. (b) Barker, G.; Webster, S.; Johnson, D. G.; Curley, R.; Andrews, M.; Young, P. C.; Macgregor, S. A.; Lee, A.-L. *J. Org. Chem.* **2015**, *80*, 9807–9816.

(20) The autoionization (K_w) of water, pH, $\text{p}K_a$ of RB(OH)_2 , and $\text{p}K_{\text{aH}}$ of a protonated center (e.g., heterocycle) changes with temperature. Changing from H_2O to $\text{H}_2\text{O}/\text{dioxane}$ 50/50 induces $\Delta\text{p}K_a + 1$ and $\Delta\text{p}K_{\text{aH}} - 1$. See SI for discussion of K_w .

(21) Kuivila noted a slow, pH-independent hydrolysis of 2,6-dimethoxyphenyl boronic acid.^{17f} In our studies, capricious background hydrolysis occurred at neutral pH with some substrates, e.g., 1 and 2. This process was fully suppressed by addition of small amounts of chloride ion, suggesting catalysis by trace metal impurities. For systems where k_4 was a required mechanism (e.g., 5, 12–17), rates were unaffected by added chloride.

(22) (a) Brown, R. D.; Buchanan, A. S.; Humffray, A. A. *Aust. J. Chem.* **1965**, *18*, 1521–1525. (b) Deans, F. B.; Eaborn, C. *J. Chem. Soc.* **1959**, 2303–2318. (c) Florentin, D.; Fournie-Zaluski, M. C.; Callanquin, M.; Roques, B. P. *J. Heterocycl. Chem.* **1976**, *13*, 1265–1272.

(23) (a) M06L/6-311++G**, incorporating solvation free energies computed as single points employing the same level of theory and the PCM formalism.²⁴ This level gave best quantitative agreement with experiment for MIDA hydrolysis.²⁵ (b) M06/6-311+G**//B3LYP/6-31+G** was used for selected species, incorporating solvation via a single point using B3LYP/6-31+G* combined with the PCM formalism as implemented in Gaussian03;²⁶ this level was previously used for boronic acids.^{17i,27} Calculations were performed in Gaussian09 (unless noted)²⁶ at 298 K/1 atm. Ideal gas derived corrections from 1 M standard state to 25 M water gave best agreement with experiment and are used throughout. See SI.

(24) (a) Zhao, Y.; Truhlar, D. G. *Acc. Chem. Res.* **2008**, *41*, 157–167. (b) Zhao, Y.; Truhlar, D. G. *Theor. Chem. Acc.* **2008**, *120*, 215–241. (c) Tomasi, J.; Mennucci, B.; Cammi, R. *Chem. Rev.* **2005**, *105*, 2999–3094.

(25) Gonzalez, J. A.; Ogba, O. M.; Morehouse, G. F.; Rosson, N.; Houk, K. N.; Leach, A. G.; Cheong, P. H. Y.; Burke, M. D.; Lloyd-Jones, G. C. *Nat. Chem.* **2016**, DOI: 10.1038/NCHEM.2571.

(26) See SI for full citations: (a) Frisch, M. J.; et al. *Gaussian 03, Revision B.04*; Gaussian, Inc.: Wallingford, CT, 2004. (b) Frisch, M. J.; et al. *Gaussian 09, Revision C.01*; Gaussian, Inc.: Wallingford, CT, 2009.

(27) Lee, J. M.; Helquist, P.; Wiest, O. *J. Am. Chem. Soc.* **2012**, *134*, 14973–14981.

(28) Review: Renny, J. S.; Tomasevich, L. L.; Tallmadge, E. H.; Collum, D. B. *Angew. Chem., Int. Ed.* **2013**, *52*, 11998–12013.

(29) Kuivila reported added $B(OH)_3$ had no impact on rate;^{17f} however, as $[B]_{tot} \leq 5$ mM, k_{2cat} would be negligible.

(30) Marshall, W.; Franck, E. *J. Phys. Chem. Ref. Data* **1981**, *10*, 295–304.

(31) Cole, T. E.; Haly, B. D. *Organometallics* **1992**, *11*, 652–657.

(32) Formally, the lower free energy boroxine-ate complexes provide the reference points for these reactions. However, for ease of comparison, the boronates are retained as zero point.

(33) As far as we are aware, $R_3B/RB(OH)_2$ interconversion by a nonoxidative aqueous basic pathway has only been implicated as a side reaction in oxidation of 1,1-diboryl alkanes: Brown, H. C.; Zweifel, G. *J. Am. Chem. Soc.* **1961**, *83*, 3834.

(34) (a) pK_{aH} 15–17: Sadler, S. A.; Tajuddin, H.; Mkhaliid, I. A. L.; Batsanov, A. S.; Albesa-Jove, D.; Cheung, M. S.; Maxwell, A. C.; Shukla, L.; Roberts, B.; Blakemore, D. C.; Lin, Z.; Marder, T. B.; Steel, P. G. *Org. Biomol. Chem.* **2014**, *12*, 7318–7327. (b) pK_{aH} 8: Lezina, V. P.; Kozlova, M. M.; Gashev, S. B.; Stepanyants, A. U.; Smirnov, L. D. *Chem. Heterocycl. Compd.* **1986**, *22*, 903–914. (c) pK_{aH} 6, 13, 14: Brisset, J.-L.; Ilimbi, V. *Can. J. Chem.* **1980**, *58*, 1250–1252.

(35) For processes that only impact at pH extremes (e.g., k'_3, k'_5) or where the heterocycle $pK_{aH} < 1$, the values are overestimates.

(36) (a) Geissler, P. L.; Dellago, C.; Chandler, D.; Hutter, J.; Parrinello, M. *Science* **2001**, *291*, 2121–2124. (b) Gunaydin, H.; Houk, K. N. *J. Am. Chem. Soc.* **2008**, *130*, 15232–15233.

(37) Beno, B. R.; Yeung, K.; Bartberger, M. D.; Pennington, L. D.; Meanwell, N. A. *J. Med. Chem.* **2015**, *58*, 4383–4438.

(38) For generation of 2-pyridinium-carbenoids, see: Ratts, K. W.; Howe, R. K.; Phillips, W. G. *J. Am. Chem. Soc.* **1969**, *91*, 6115–6121.

(39) For a related mechanistic proposal involving ylide liberation from the conjugate base of 2-pyridinium boronic acid (formal prototropy), see: Fuller, A. A.; Hester, H. R.; Salo, E. V.; Stevens, E. P. *Tetrahedron Lett.* **2003**, *44*, 2935–2938.

(40) Ji, L.; Edkins, R. M.; Sewell, L. J.; Beeby, A.; Batsanov, A. S.; Fucke, K.; Drafz, M.; Howard, J. A. K.; Moutounet, O.; Ibersiene, F.; Boucekkine, A.; Furet, E.; Liu, Z.; Halet, J.-F.; Katan, C.; Marder, T. B. *Chem. - Eur. J.* **2014**, *20*, 13618–13635.

(41) (a) Li, Y.; Asadi, A.; Perrin, D. M. *J. Fluorine Chem.* **2009**, *130*, 377–382. (b) Yan, J.; Springsteen, G.; Deeter, S.; Wang, B. *Tetrahedron* **2004**, *60*, 11205–11209.

(42) (a) Li, H.; Zhong, Y.-L.; Chen, C.-y.; Ferraro, A. E.; Wang, D. *Org. Lett.* **2015**, *17*, 3616. (b) Chen, X.; Ke, H.; Chen, Y.; Guan, C.; Zou, G. *J. Org. Chem.* **2012**, *77*, 7572. (c) Haag, B. A.; Sämman, C.; Jana, A.; Knochel, P. *Angew. Chem., Int. Ed.* **2011**, *50*, 7290. (d) Winkle, D. D.; Schaab, K. M. *Org. Process Res. Dev.* **2001**, *5*, 450.

(43) For $\geq 10\%$ of maximum biomolecular reactivity ($\geq 2.5\%$ minor species), $\log[97.5/2.5] = 1.6$; thus, $pH = pK_a \pm 1.6$

(44) (a) Molander, G. A.; Canturk, B.; Kennedy, L. A. *J. Org. Chem.* **2009**, *74*, 973–980. (b) Ren, W.; Li, J.; Zou, D.; Wu, Y.; Wu, Y. *Tetrahedron* **2012**, *68*, 1351–1358.